Evaluation of arc quenching characteristics of various gases using power semiconductors

doi: 10.1088/1361-6463/aa8f8a

Evaluation of arc quenching characteristics of various gases using power semiconductors

Tomoyuki Nakano[1]†, Yasunori Tanaka[1]‡, K Murai[1], Y Uesugi[1], T Ishijima[1], K Tomita[2], K Suzuki[3], T Shinkai[4]

[1]Division of Electrical Engineering and Computer Science, Kanazawa University, Kakuma, Kanazawa 920-1192, Japan
[2]Kyushu University, Kasuga, Fukuoka, JAPAN
[3]Tokyo Denki University, Tokyo, JAPAN
[4]Tokyo University of Technology, Tokyo, JAPAN

E-mail: tnakano@stu.kanazawa-u.ac.jp,tanaka@ec.t.kanazawa-u.ac.jp

Abstract. This paper presents the arc quenching abilities of various gases studied using a power semiconductor switching technique. This technique uses an insulated gate bi-polar transistor (IGBT) for current injection and voltage application to the arc plasma. Using this technique, arcs under a free recovery condition from a 50 A steady state condition were investigated in SF_6, CO_2, O_2, N_2, air and Ar gas flows. Furthermore, at a specified timing, high of voltage about 1.1 kV and 1.7 kV/μs was applied by the IGBT to residual decaying arcs to elucidate the arc re-ignition processes and recovery properties. These systematic experiments further enabled us to estimate the interruption probability versus the voltage application timing. From these results, the voltage application timing of 50% successful interruption was estimated for various gases. The results showed a direct relation to the interruption capabilities of the respective gases. These results were then compared to electron density measurement results and numerical simulation results to confirm their validity. All data obtained from experiments and simulation are expected to be useful to elucidate the arc quenching physics and also for the practical application of arc quenching phenomena.

Submitted to: *J. Phys. D: Appl. Phys.*

† To whom correspondence should be addressed (tnakano@stu.kanazawa-u.ac.jp)
‡ To whom correspondence should be addressed (tanaka@ec.t.kanazawa-u.ac.jp)

1. Introduction

A gas circuit breaker uses SF_6 gas as an arc quenching medium because SF_6 gas has quite high arc-quenching ability and current interruption ability. However, SF_6 has been specified as a greenhouse gas because it has a 22 800 times higher global warming potential (GWP) than CO_2 has. Consequently, it is necessary to reduce the amounts of SF_6 released to the atmosphere by reducing the amounts of SF_6 that are used. One solution for reduction of SF_6 use is to develop alternative gases for SF_6. Some alternative candidates have been investigated to date, such as high pressure CO_2, CO_2-CF_3I, CO_2-CH_4, and N_2-H_2 [1, 2, 3, 4]. Recently, fluoronitrile-CO_2 mixture and fluoroketone-CO_2 mixture has been proposed as alternatives to SF_6 [5, 6]. Other approaches to reduce the amount of SF_6 use are to reduce the GCB size with less deterioration of the interruption ability. To substitute SF_6 with alternative materials or to reduce the GCB size, detailed understanding of residual arc properties in the current interruption process is fundamentally important.

The authors have been investigating decay processes of gas-blast arcs fundamentally using both numerical [7, 8] and experimental approaches. For the experiment, we have developed a simple arc device [9]. In the device, an arc plasma can be established between the moving electrode and the fixed electrode in the nozzle space. As a power source, a DC current source has been set up. Its output current can be switched using a power semiconductor, e.g. insulated gate bipolar transistor (IGBT). The use of IGBT can control the arc current injection or voltage application accurately within a microsecond. By adopting time-accurate control of the current injection and voltage application, we measured the electron density in arcs around current zero and under free recovery conditions in a gas flow using laser Thomson scattering (LTS) [10, 11] and Shack–Hartmann type laser wavefront sensors [12]. In addition to these, we have developed a new fundamental investigation technique for arc behaviours during the re-ignition process [13, 14, 15]. This technique uses IGBTs to control not only the arc current but also applied voltage with high accuracy in a time domain. Using the technique, transient voltage can be applied intentionally between the electrodes at specified timing under the free recovery condition. This applied voltage is called "quasi-transient recovery voltage (quasi-TRV)" because it is generated artificially. By application of this quasi-TRV, we can study arc re-ignition processes and recovery properties in a thermal mode.

In this work, we systematically obtained the arc quenching properties of SF_6, CO_2, O_2, N_2, air, and Ar using the developed technique [13]. A direct current 50 A arc was ignited in each gas flow at a given flow rate in the nozzle space and was sustained in a steady state. Subsequently, the arc current was commutated by IGBT from the arc plasma to the IGBT to produce the arc under free recovery condition. The arc decay process under the free recovery condition is the most basic property for arc-interruption phenomena. Arc behaviours in a steady state and in a decaying phase were observed using a high-speed video camera. Furthermore, we found the systematic data on the

interruption probability of each gas as a function of the timing of quasi-TRV application through more than 10–30 shots, which can be regarded as the recovery properties in a thermal mode. Electron density measurements were also taken at the nozzle throat using LTS to study arc decaying processes in various gas flows. In addition, numerical simulation was undertaken to investigate the temperature decay process of the arc under a free recovery condition for various gases. All data obtained from the experiments and simulation will be useful to elucidate the arc quenching physics and also for practical application of arc quenching phenomena.

2. Experimental setup

2.1. Electric circuit for current injection and voltage application

Figure 1 depicts the electrical circuit used for this work. The electric circuit has a direct current (dc) source, an IGBT element, and an arc device. The dc current source is an inverter type of dc current source rated at 150 A and 250 V. This dc current source is connected in series to the arc device to sustain an arc discharge between the electrodes in the arc device. To the electrodes, an IGBT element ($IGBT_p$) is connected in parallel. Switching-on this $IGBT_p$ can commutate the arc current from the arc discharge between the electrodes to the $IGBT_p$. This switching-on the $IGBT_p$ creates a free recovery condition between the electrodes, in which the arc discharge decays with time without current injection and voltage application. In addition, at the specified timing during arc decay, switching-off the $IGBT_p$ can apply the source voltage again to the decaying arc discharge between the electrodes. At that time, a steep voltage from the current source is applied respectively between the electrodes with a peak and a rise rate of 1.1 kV and 1.7 kV/μs, respectively. This applied voltage is called 'quasi-transient recovery voltage (quasi-TRV)' because it is similar to a regular TRV, but it is artificially generated. One feature of the use of the IGBT element is that it can provide high time accuracy to create the current commutation for a free recovery condition and the application of quasi-TRV. The IGBT element has a short response time and jitter of less than 1.0 μs. Therefore, we can apply the quasi-TRV to the decaying arc discharge at the specified delay time t_d from initiation of the arc decay.

When the quasi-TRV is applied during the arc decay, then the arc plasma is re-ignited in some conditions. This arc re-ignition is regarded as a current interruption failure. If the arc plasma continues to decay in spite of the quasi-TRV application and the current converges to zero, then this situation is regarded as a successful interruption. The probability of the successful interruption depends on the delay time t_d for quasi-TRV application. In addition, this successful interruption probability versus t_d is strongly dependent on the gas species, the gas flow rate, and other factors that determine the arc quenching ability. The voltage between the electrodes was measured using a CR potential divider. The source current, the arc current, and the IGBT current were measured respectively using current transformers.

2.2. Configuration of the arc device and the nozzle

Figure 2 depicts the configuration of the arc device used in this work. The arc device consists of a vacuum chamber, a moving electrode and a fixed electrode, and a nozzle for gas flow. The outer diameter of the chamber is 200 mm. The upper electrode, which works as the anode, is the moving electrode driven by a compressed air cylinder. The lower electrode works as the cathode. It is the fixed electrode. These electrodes are surrounded by a gas-blast nozzle.

Figure 3 presents a schematic diagram of the nozzle and the electrodes, and a photograph of the nozzle made of transparent polymethylmethacrylate (PMMA). The electrode tips are made of copper tungsten (70%Cu-30%W). The moving electrode has 6 mm body diameter and 3 mm tip diameter. The body diameter and the tip diameter of the fixed electrodes are, respectively, 30 mm and 10 mm. The gap separating these electrodes has a distance of 50 mm at a full open position. These electrodes are surrounded by the nozzle. The gas inlet diameter is 40 mm, whereas that of the outlet is 18.75 mm. This nozzle has a throat with 10 mm diameter and 10 mm length. We used nozzles made of polytetrafluoroethylene (PTFE) for arc tests. For observation of arc behaviour in the nozzle only, a nozzle made of transparent PMMA was used.

2.3. Experimental arrangements for Laser Thomson scattering method

Laser Thomson scattering (LTS) is widely used for precise measurements of electron density in arc plasmas. When a laser light is injected to an arc plasma, free electrons in the arc plasma are excited by electromagnetic field of the laser light, resulting in the light scattering. This is called Thomson scattering. One of the characteristics of LTS measurement is that it can measure local values of electron density and electron temperature without local thermodynamic equilibrium (LTE) assumption [16]. Details for LTS measurements have already been described for this system in our previous literature [10].

Electron density in the arc near the nozzle throat is a key physical parameter to ascertain arc interruption phenomena. The electron density at the nozzle throat was measured using LTS method. One characteristic of LTS measurement is that it can measure local values of electron density and electron temperature without a local thermodynamic equilibrium (LTE) assumption [16]. For LTS measurement, the second harmonic of an Nd:YAG laser at a wavelength of 532 nm was used. The pulse width of the laser beam was 10 ns. The laser energy was 200 mJ. Figure 4 shows an image of the PTFE nozzle for LTS measurement and schematic cross sections of the nozzle. As this figure shows, the PTFE nozzle has a hole with 3.5 mm $\times$ 3 mm and a hole 10 mm $\times$ 3 mm for LTS measurement. These holes are positioned at the nozzle throat, which is at a height of 28 mm from the lower electrode surface. These two holes are arranged in a horizontal direction and are mutually perpendicular. The smaller hole is for the incident laser beam path. The larger hole is for observation of 90^{o} scattered laser light. The laser beam has a focused spot diameter of less than 0.5 mm. However, the laser

beam size is spread intentionally in the horizontal direction using a cylindrical lens to have 4.5 mm width. The horizontally spread laser beam is used because the laser beam can be irradiated to the arc column even if the arc axis is shifted from the nozzle axis. The arc plasmas in SF_6 or CO_2 flow are well known to be unstable and to fluctuate. The larger hole was covered with glass plates to prevent hot gas ejection from the holes. The covering hole by glass plates reduced influences of the hole on the arc behaviours.

3. Experimental measurements

3.1. Experimental condition and procedure

We used gases SF_6, CO_2, O_2, N_2, air, and Ar with a 100 L/min flow rate which corresponds to a gas flow velocity of 1.768 m/s at the nozzle inlet, and SF_6 and CO_2 with a 50 L/min flow rate which corresponds to a gas flow velocity of 0.884 m/s at the nozzle inlet. The electric arc current was fixed at dc 50 A. The pressure inside the chamber and the nozzle at the initiation of an arc discharge was set to 0.1 MPa. The arc behaviour was observed using a high-speed video camera. Its frame rate was set to 300 000 frames/s. The exposure time was 1.0 μs. The PMMA nozzle was used only for the high-speed video camera observation. In other experiments, the PTFE nozzle with holes was used for LTS measurement and also for evaluation of the arc quenching ability of the gases. We measured the output current of the dc current source (i_{source}), the current between the electrodes (i_{arc}), the current in $\mathrm{IGBT_p}$ (i_{IGBT}), the voltage between the electrodes (V_{arc}), and the $\mathrm{IGBT_p}$ gate voltage and the electrode driving voltage.

We measured the arc current, the IGBT current, the source current, and the voltage between the electrodes. Figure 5 presents an example of the measured current and voltage waveforms through one experiment. The experimental procedure is explained below.

(i) Before the experiment, the electrode is closed by supplying ac 100 V of the electrode driving voltage, as shown in panel (f). The $\mathrm{IGBT_p}$ is switched off, which can be done by application of the gate voltage of −15 V as shown in panel (e).

(ii) The chamber including the arc device is evacuated using a vacuum pump to reduce the pressure inside the chamber to about 50 Pa. Subsequently the valve between the chamber and the vacuum pump is shut.

(iii) Gas is supplied from the lower part of the chamber at specified inlet flow velocity: 1.768 m/s (= a gas flow rate of 100 L/min) or 0.884 m/s (=50 L/min).

(iv) When the pressure inside the chamber reaches 0.1 MPa, the electric source current of 30 A is supplied to the closed electrodes for 100 ms. This process is shown at t=−0.47 s to −0.37 s in panels (a) and (b) of figure 5. Subsequently, the current source increases the current from 30 A to 50 A in 20 ms, corresponding to waveforms from t=−0.37 s to −0.35 s in panels (a) and (b).

(v) At 120 ms after the current reaches 50 A, the upper electrode is initiated to open by stopping application of the electrode driving voltage as presented in panel (f). The duration of 80 ms is necessary for the moving electrode for its full opening stroke. At this time, the arc plasma is established between the electrodes. The arc voltage is increased with the stroke.

(vi) After opening the electrode, arc plasma of dc 50 A is sustained in 160 ms between the electrodes. Then, the arc voltage becomes stable in this steady state. One can find the stable arc voltage in time from -0.1 s to 0 s in panel (d). From this time region, the arc is observed using a high-speed video camera.

(vii) At t=0 s, the $\mathrm{IGBT_p}$ is switched-on to commutate the source current from the arc plasma to the $\mathrm{IGBT_p}$. As a result, the arc current and arc voltage smoothly decrease respectively to 0 A and 0 V. leading to the so-called free recovery condition.

(viii) After a specified delay time t_d from the $\mathrm{IGBT_p}$ switching-on, the $\mathrm{IGBT_p}$ is switched-off again. This switching-off of the $\mathrm{IGBT_p}$ applies a quasi-TRV to the electrodes. If the arc current increases between the electrodes after quasi-TRV application, then we judge the arc re-ignition and the current interruption failure. If the arc current continues to decrease to 0 A, then we judge the successful current interruption. In this work, t_d can be set from 10 μs to 500 μs.

(ix) After 1.0 ms from initiation of quasi-TRV application, the $\mathrm{IGBT_p}$ is switched on again to commutate the current from the arc plasma to the IGBT.

(x) The current source is turned off to halt the experiment.

This experimental procedure provides (I) a gas blast arc sustained in a steady state, (II) free recovery condition generated using the IGBT control, (III) application of quasi-TRV to the electrodes, and (IV) judgment between the success or failure of current interruption.

3.2. Application of quasi-transient recovery voltage to gas-blast arcs under a free recovery condition

Figures 6 and 7 respectively present the conceptual diagram of the source current, the arc current, and the voltage between the electrodes, in cases of successful interruption and arc re-ignition. These figures include only the waveforms around the current commutation and quasi-TRV application. Successful interruption is recognized when the electric current continues to decrease even after quasi-TRV application. However, if the current increases through the residual arc after quasi-TRV application, it is recognized as the interruption failure or arc re-ignition. From the waveforms of the current and voltage between the electrode, one can judge successful interruption and interruption failure clearly. Furthermore, changing the delay time t_d enables us to investigate the dielectric recovery property between the electrodes. At the same time, arc behaviour was observed using a high-speed video camera to study the arc decay and the position of the electrical breakdown between the electrodes.

It is necessary to fix the quasi-TRV waveform for comparison. Figure 8 presents the prospective waveform of quasi-TRV. The vertical axis shows voltage between the electrodes. The horizontal axis presents time from initiation of a quasi-TRV application. The prospective quasi-TRV is an oscillating voltage governed by inductance in the dc current source and a strayed impedance in the circuit. The first peak of the quasi-TRV reaches 1.1 kV. Its rise rate is 1.7 kV /μs. In this work, the quasi-TRV is applied to an arc plasma under a free recovery condition.

4. Experimental results

4.1. Arc shape and arc voltage in a steady state before the free recovery condition

Before describing arc decaying processes under free recovery condition, we show the arc behaviour under a steady state condition before the free recovery condition because arc stability under a steady state condition with a gas flow is fundamental and is then also related to the arc behaviour under a transient condition.

Figure 9(a) depicts arc behaviour in a steady state in SF_6 with inlet flow velocity of 1.768 m/s (= a gas flow rate of 100 L/min) and 0.884 m/s (=50 L/min). The shape of the nozzle and the electrodes are drawn with white lines. The gas inlet is located at the bottom of the figure. Each image is captured by a high speed video camera with a sensitivity for visible light in a wavelength range from 400 to 800 nm. Originally, the radiation of visible light from the arc is expressed as a monochrome image signal with a depth of 8 bits = 256 levels. We have converted this monochrome image signal to coloured image signal according to the magnitude of radiation intensity. Here, the red colour corresponds to high intensity and the blue indicates low intensity. The images shown here are colour maps on a logarithmic scale. The images include timings of photographs on the bottom of the figure. The time base is equivalent to that of figure 5. As the pictures show, the SF_6 arc has a frequently changed shape in the nozzle space, even with spiral shapes for 1.768 m/s and 0.884 m/s. This shape instability of the arc might originate from the turbulent flow because of SF_6 characteristics. Generally, SF_6 has a heavy mass density and a high Reynolds number (Re), that can be written as

$$Re = \frac{\rho u L}{\mu} \tag{1}$$

where ρ is the mass density of the gas, u is the velocity of the gas flow, μ is the viscosity of the gas, and L is a characteristic length like the size of the gas flow inlet. Higher Reynolds number of SF_6 gas flow with higher mass density is thus subject to the production of turbulent flows. Furthermore, SF_6 can be dissociated thermally to SF_4, SF_2, SF, respectively, at 1800 K, 2000 K and 2200 K involving local expansion and also causing turbulent flow. These dissociations also offer a high specific heat and thermal conductivity of SF_6, leading to a high arc quenching ability, which also might make the arc discharge unstable and fluctuating. The arc current and voltage in the steady state are presented in figure 10(a) for SF_6 gas inlet flow velocity of 1.768 m/s and 0.884 m/s.

The upper panel presents the arc current. The lower panel presents the arc voltage. As shown there, the arc current was almost constant around dc 50 A. The arc voltages fluctuate considerably, especially for the case of 1.768 m/s inlet flow velocity. The arc voltage fluctuation is attributable to arc length fluctuation by turbulent flow. In spite of that, we can sustain these SF_6 arcs at 50 mm length.

The arc behaviours in CO_2 gas flow were also measured as depicted in figure 9(b) for inlet flow velocity of 1.768 m/s and 0.884 m/s. The CO_2 arc is also bent with 1.768 m/s inlet flow, not markedly compared to SF_6 arcs. However, the CO_2 arc with 0.884 m/s inlet velocity has a straight stable shape. This stability can be confirmed in the measured arc voltage, as presented in figure 10(b). As the figure shows, the arc voltage for 0.884 m/s inlet flow velocity is absolutely stable around 120 V, whereas the arc voltage with 1.768 m/s inlet flow velocity shows random fluctuation. CO_2 has relatively higher density than air and N_2, but it is quite lower compared to that of SF_6. Only the higher inlet flow velocity can cause appearance of turbulent effects for CO_2 arcs.

The arc behaviours in a steady state are presented in figure 11 in O_2, N_2, air, and Ar with 1.768 m/s inlet flow velocity. As shown in this figure, arcs in these gas flows have quite a straight shape stably. Moreover, it is well controlled with almost no fluctuation. The main difference between these gas arcs is the diameter of the arcs. The Ar arc has the largest diameter among the gases. The second largest arc is the O_2 arc. The N_2 and air arcs seem to have similar diameters. The Ar arc has the largest diameter because Ar has noble gas without dissociations leading to energy consumption and then shrinkage of the arc plasma. Figure 12 presents the arc current and voltage in O_2, N_2, air, and Ar with 1.768 m/s inlet flow velocity. The arc voltage waveform in each gas is stable only with voltage fluctuation from the inverter current output. The N_2, air and O_2 arcs have similar arc voltage of around 110–130 V. That of O_2 is slightly lower than that of either N_2 or air. The arc voltage of Ar is about 50 V. It is markedly lower than others. In terms of passage diameter of the current, these results of the arc voltage show good agreement with the observed arc diameters shown in figure 11.

4.2. Dynamic arc behaviours in the decaying phase

Figure 13(a) depicts the arc behaviour in a decaying phase under free recovery conditions in SF_6 gas flow at inlet flow velocity of 1.768 m/s. This figure presents images taken at the timing t of 0, 3.3, 6.7, 10, 20 and 30 μs from the initiation of the arc decay. As the pictures show, the SF_6 arc discharge decays with time, keeping its shape at time 0 μs. The radiation intensity from the SF_6 arc decreases almost uniformly along the arc, roughly speaking, although some parts, between the lower electrode and the nozzle throat inlet for example, decline more rapidly. As a result, at t=20 μs, the radiation from the arc becomes very weak, remaining downstream of the nozzle throat in this case. Furthermore, at t=30 μs, the arc plasma has weak radiation in the nozzle space. If we use SF_6 with the inlet flow velocity of 0.884 m/s, then the arc behaviour is distinctive, as depicted in figure 13(b). In this case, the arc plasma also decays over the entire part

of the nozzle space with a slightly lower decay rate than that at 1.768 m/s. However, one distinct feature is the local rapid decay in the arc plasma along the arc. In spite of that, rapid decay in the radiation intensity between the lower electrode and the nozzle throat is obtainable. Such a reduction and local rapid decay along the arc plasma are attributed to a high arc quenching ability of SF_6 and turbulent effects.

In the case of CO_2, local decay from the gas flow around the nozzle throat is apparent. Figure 14 presents the arc behaviour in a decaying phase in CO_2 with inlet flow velocity of 1.768 m/s and 0.884 m/s. For both cases, CO_2 arc decay was initiated near the nozzle throat. Fast decay around the nozzle throat is apparent, especially in the case of 1.768 m/s. At t=6.7 μs, the radiation intensity around the upper side of the nozzle throat already became much weaker than other parts. At t=30 μs, the intensity also at the lower side of the nozzle throat decreases with time. As this figure shows, the CO_2 gas flow enhances the arc plasma decay around the nozzle throat, which implies the importance of the nozzle throat for CO_2 arc decay. This tendency is also apparent in case of 0.884 m/s inlet flow velocity, but the decay rate at 0.884 m/s is much lower than that at 1.768 m/s.

The arc behaviours in decaying phase in O_2, N_2, air and Ar are obtainable in figure 15 at inlet flow velocity of 1.768 m/s. The arc decaying process depends on the gas kinds markedly. The O_2 arc still has a high radiation intensity at t=10 μs, whereas the radiation intensity from the N_2 and air arcs decreases faster than that of O_2 arcs. Through a test, a nozzle burned with a flame in a case of O_2 gas introduction. It would be thus possible that combustion of ablation vapour restrains a decrease in radiation intensity from O_2 arcs. Similarly, the radiation intensity from the air arc is comparably higher than that of the N_2 arc at 30 μs. For O_2, N_2 and air arcs, the arcs decline remarkably around the nozzle throat. The Ar arc shows a gradual and slow decay in the radiation intensity.

High-speed video camera observations confirmed that the nozzle throat plays important roles in arc decay in most cases. At the nozzle, cold gas from the inlet is blown directly to the arc plasma, which results in high convection loss to reduce the arc diameter; then a high thermal conduction loss there. However, those effects on decaying arcs in each gas mutually differ. Such behaviour is obtainable by numerical simulation, as described in a later section.

4.3. Probability of successful interruption versus quasi-TRV application

One important feature of our experimental tests is to estimate arc interruption ability by application of quasi-TRV in the fixed conditions. In a free recovery condition, quasi-TRV was applied by switching off the IGBT again at a specified delay time t_d. This test was applied to investigate the recovery properties of the space between the electrodes.

Figure 16 presents the IGBT signal, the arc current, and the arc voltage for a SF_6 arc with 1.768 m/s inlet flow velocity for t_d=20 μs. The arc current is commutated to the IGBT at t=0 μs by switching on the IGBT. In this case, the arc current has a finite

current decay rate di/dt because it requires a finite time for transition of IGBT from off-state to on-state, and circuit inductance. At t_{d}=20 μs, the IGBT is switched off again to apply source voltage of 1.1 kV with a rise rate of 1.7 kV/μs between the electrodes. As panel (a) shows, the arc current continues to decrease to 0 A with time, which is regarded as successful interruption. Panel (b) depicts the waveforms in the interruption failure case, although the same delay time t_{d}=20 μs for quasi-TRV application was used. In this figure, the arc current again increases to 50 A through arc re-ignition at applied voltage of 0.75 kV. This interruption failure seems to be a thermal failure or a failure in a thermal mode, not in a dielectric mode, because the arc current increases gradually with time during 8 μs. Generally in a dielectric mode, the current jumps up with a voltage drop at the arc re-strike. In this way, successful interruption occurs with a certain probability. If the delay time t_{d} for quasi-TRV application is sufficiently long, then the probability of successful interruption reaches 100%. When t_{d} is short, the arc is always re-ignited easily between the electrodes.

Figure 17 presents the experimentally obtained probability of successful interruption in a thermal mode versus the delay time t_{d} for quasi-TRV application. This figure includes results for inlet flow velocity of 1.768 m/s. Each of the probabilities was obtained through 10–40 shots for each condition. As this figure shows, SF_6 requires a delay time t_{d} less than 28 μs for quasi-TRV application to prevent arc re-ignition in thermal mode. In other words, a shorter t_{d} than 20 μs engenders arc re-ignition. In addition, an important matter for SF_6 is that the interruption probability increases extremely with t_{d} from 20 to 30 μs. That point above implies an extremely high arc interruption ability in a thermal mode and remarkably rapid recovery of SF_6 against voltage application. In other words, a SF_6 residual arc under a free recovery condition can lose its electrical conductivity at a point or points along the arc discharge between the electrodes. As a result, the delay time $t_{\mathrm{d50\%}} = 28$ μs obtains 50% successful interruption, where the $t_{\mathrm{d50\%}}$ is defined as t_{d}, with which the interruption probability becomes 50%.

For other gases, much longer t_{d} is necessary for quasi-TRV application without arc re-ignition, compared to t_{d} for SF_6. The CO_2 and O_2 shows similar results for the interruption probability versus t_{d}. Therefore, these gases have similar recovery properties in thermal mode. For CO_2 and O_2, the quantity $t_{\mathrm{d50\%}}$ can be estimated as 108 μs. Air and N_2 gases require longer t_{d} for successful interruption in thermal mode. The delay times for 50% successful interruption $t_{\mathrm{d50\%}}$ were estimated as 190 μs for air and as 230 μs for N_2. It is reasonable that air shows results that are intermediate between N_2 and O_2 because air is a mixture of 78%N_2 and 22%O_2. However, Ar has an extremely long $t_{\mathrm{d50\%}}$ of 480 μs, which indicates very slow recovery of Ar for electrical conductivity. This result is consistent with the fact that Ar is used widely as working gas for plasma applications for stable plasma sustainment.

The successful interruption property is related to recovery properties in a thermal mode, which depends on the decay rate in the electrical conductivity. The decay rate in the electrical conductivity is directly connected to decay in the electron density, and

to the temperature. The temperature decay at the nozzle throat is again influenced by the gas flow convection loss with high specific heat at low temperature $\rho C_{\mathrm{p}} \boldsymbol{u} \cdot \nabla T$ and the thermal conduction $\nabla \cdot \kappa \nabla T$, where ρ is the mass density, C_{p} denotes the specific heat, $\boldsymbol{u}$ represents the gas flow velocity, κ is the thermal conductivity, and T is the temperature. The gas SF_6 has a higher specific heat ρC_{p} and thermal conductivity κ at low temperatures of about 1800, 2000 and 2200 K, arising from dissociation–association reactions from SF_6 to SF_4, SF_4 to SF_2, and SF_2 to S and F. This higher specific heat and thermal conductivity are favourable for decay of the temperature and electrical conductivity.

Such a successful interruption probability versus t_{d} can be adopted for different gas conditions such as gas flow rates. Figure 18 presents the probability of successful interruption versus t_{d} for SF_6 and CO_2 at two different inlet gas flow velocities of 1.768 m/s and 0.884 m/s. Open squares represent the results for 1.768 m/s SF_6 gas introduction. Open squares with a cross correspond to 0.884 m/s SF_6 gas introduction. Similarly, results for 1.768 m/s CO_2 gas introduction are shown by open triangles. Triangles with a cross are for 0.884 m/s CO_2 gas introduction. For SF_6 gas flow, the increase rate in the successful interruption probability versus t_{d} is rather gradual at 0.884 m/s compared to 1.768 m/s. As a result, $t_{\mathrm{d50\%}}$ is estimated as 40 μs for SF_6 at 0.884 m/s, which is 1.4 times as long as $t_{\mathrm{d50\%}}$ at 1.768 m/s. This result suggests a quantitative reduction in the interruption ability in a thermal mode by a decrease in the gas inlet flow velocity for SF_6. The interruption ability of CO_2 was also degraded by a decrease in the gas inlet flow velocity. Actually, the quantity $t_{\mathrm{d50\%}}$ becomes 150 μs for CO_2 at 0.884 m/s, which is 1.4 times as long as $t_{\mathrm{d50\%}}$ at 1.768 m/s. This result might imply that a decrease in gas inlet flow velocity from 1.768 to 0.884 m/s reduces the recovery rate similarly for SF_6 and CO_2.

The successful interruption probability versus the delay time t_{d} for voltage application was obtained systematically.

It is noted that the relationship between interruption probabilities versus t_{d} in figures 17 and 18 is just a relative relationship for different gas kind conditions and gas flow rates at a fixed TRV application. If we use higher TRV application, the results of figures 17 and 18 would be shifted to longer delay time side. This means that, longer time is needed for the space between the electrodes to recover enough to withstand higher TRV application. Nevertheless, we could compare a relative relationship for different gas kinds and different gas flow rates. SF_6 could need only a shorter delay time for current interruption compared to the other gases because of SF_6's rapid recovery property. These data include useful information and contribute to the elucidation of arc interruption phenomena for fundamental and practical sides.

4.4. Waveforms of current and voltage on interruption failure

The experiment results revealed some interruption failure cases at the critical t_{d}. Figure 19 presents the waveforms of current and voltage on the interruption failure

at the 1.768 m/s gas introduction. The upper panel presents the voltage between the electrodes. The lower panel presents the arc current. The horizontal axis shows the time from the initiation of quasi-TRV, t' in this figure. All waveforms were acquired as a 'failure case' with quasi-TRV application at nearly $t_{\mathrm{d50\%}}$, i.e. t_{d}, which provides 50% probability of successful interruption for each gas.

Figure 19(a) shows the current and voltage after quasi-TRV application at t_{d} of 30 μs for SF_6 at the 1.768 m/s gas introduction. In this case, the arc current started increasing just from $t' = 2$ μs. The voltage dropped, which means that the SF_6 arc was re-ignited almost at t'=2 μs. In this way, SF_6 arc re-ignition mostly occurs before the first peak of quasi-TRV, which might be attributable to the fact that the residual SF_6 arc channel remained at a high temperature and became conductive again because of joule heating by a small current injection. Otherwise the arc re-ignition is avoided by rapid quenching of SF_6. Therefore, the thermal mode determines the success or failure of current interruption at $t_{\mathrm{d}} = 30$ μs for SF_6.

Arc re-ignition occurs in CO_2 gas at 1.768 m/s inlet flow velocity as presented in figure 19(b) for $t_{\mathrm{d}} = 110$ μs. In this case, the arc was re-ignited at more than 5 μs after quasi-TRV application initiation. Many cases show such microsecond arc re-ignition for $t_{\mathrm{d50\%}}$ TRV application. In this figure, current of less than 5 A can be confirmed to flow immediately before the rapid increase in current. This result suggests that the residual CO_2 arc became conductive gradually because of joule heating caused by a small current after quasi-TRV application in a thermal mode. Figure 19(c) depicts the result for N_2 gas at 1.768 m/s and $t_{\mathrm{d}} = 240$ μs. In this case, the arc was re-ignited more than 10 μs after quasi-TRV application. Furthermore, the arc current increases and the voltage drops after re-ignition slowly because the electrical conductance change in N_2 arc was very slow in this case. From the results described above, it was also inferred that SF_6 gas has extremely high arc-quenching performance and high post-arc current withstand capability, and that CO_2 gas has medium quenching ability and post-arc current withstand capability, compared to N_2.

5. Discussion

5.1. Electron density measured using laser Thomson scattering

Through the current interruption tests, the electron density of the arc in decaying process was measured using the laser Thomson scattering (LTS) method [10, 11]. This section presents a description of a part of the measured electron density for consideration of current interruption capabilities of SF_6, CO_2, and N_2.

Figure 20 presents time evolutions in the electron density in SF_6, CO_2, and N_2 residual arcs under free recovery conditions at 1.768 m/s gas introduction. The LTS measurement was done at the nozzle throat outlet, as shown in figure 4. The nozzle throat is regarded as an important location for arc-quenching phenomena. Results for 3–5 shots were derived at each timing and for each kind of gas. A mean value and

maximum and minimum values are shown with error bars in the figure. Before t=0 μs in this figure, the arc plasma is established using dc current of 50 A. At t=0 μs, the electron density n_e is 6.0 $\times$ 10^{22} m^{-3} for SF_6 and CO_2, whereas n_e is estimated as 10.0 $\times$ 10^{22} m^{-3}. After current decreases to 0 A at t >0 μs, the electron density decreases rapidly with time. In N_2 gas, the electron density decreases gradually with time to reach 0.3 $\times$ 10^{22} m^{-3}. SF_6 and CO_6 cause a rapid decrease in the electron density with time. At t=20 μs, the electron densities for SF_6 and CO_2 become 1.1 $\times$ 10^{22} m^{-3}. Additionally, it is noteworthy that the electron density in SF_6 could not be determined from LTS at t > 20 μs because the electron density might decay to its lower limitation of <10^{21} m^{-3} detectable by LTS. This fact suggests a remarkable decay ability of SF_6 for the electron density at t >20 μs compared to CO_2 and N_2.

These results of decay in the electron density show good agreement with the results on radiation intensity in arcs observed from high-speed video camera observation. As shown in figure 13, at t=0 μs, the shape of SF_6 arc tends to be a spiral. After current down to 0 A at t >0 μs, the entire part of the residual SF_6 arc quickly decays simultaneously. Then the overall decay with some local decay in the residual arc can also be obtained at t > 20 μs. This quick decay of SF_6 arcs agrees with a rapid decay in the electron density shown in figure 20. However, the shape instability of CO_2 arcs is not as high as that of SF_6 arcs, as shown in figure 14. The CO_2 arc decays more rapidly from the vicinity of the nozzle throat, which is the LTS measurement point of the electron density. Figure 20 shows that these characteristics of a CO_2 arc might cause a rapid decay in the electron density at the nozzle throat. Finally, the N_2 arc is extremely stable. It decays slowly with time, as depicted in figure 15(b). Therefore, the obtained electron density is greater and decays with time more slowly than either SF_6 or CO_2, as presented in figure 20.

As described in this section, the results of the electron density measurement fairly agree with the arc behaviour observed using a high-speed video camera. In addition, no contradiction exists with the results of current interruption tests. Nevertheless, results also show that the current interruption is determined not only at one point of the nozzle throat, especially in SF_6. Further experiments must be conducted to elucidate the arc interruption phenomena.

5.2. Transient temperature distribution of various gas arcs in nozzle by numerical simulation

In several gas conditions, the arcs decayed from near the nozzle throat. To investigate the effects of the nozzle throat on arc decay, a numerical simulation of the arc in flows of different gases was conducted [7]. Numerical simulation uses the LTE model, with the following assumptions: (1) The calculation domain is axisymmetric. (2) The arc plasma is in an LTE condition. All temperatures such as electron temperature, heavy particle temperature, and excitation temperature are equal. In addition, all reactions including dissociation/ association and ionization/ recombination take place under the

equilibrium condition. (3) The flow is laminar flow. Therefore, the turbulent effect is neglected. (4) The arc plasma is optically thin. (5) Phenomena on the electrode surface such as electron emission and ion bombardment are neglected. (6) The electric field has only an axial direction component. (7) We neglect density fluctuations caused by pressure fluctuations in a steady state, but in a transient state it is included. (8) Ablation effects of the electrodes and nozzle are neglected. (9) We consider heat conduction inside the electrodes and nozzle. Based on the assumptions presented above, we solved the conservation equations of mass, momentum, and energy as well as electromagnetic fields, together with the equation of state. Thermodynamic and transport properties of each gas were calculated in advance as functions of temperature using the calculated equilibrium composition of each gas. The program is a hand-made code based on All-speed SIMPLE algorithm reported by Patankar. Using this model, two-dimensional transient temperature and gas flow fields were calculated for SF_6, CO_2, and N_2 arcs.

Figure 21 presents the calculated two-dimensional temperature distributions of CO_2, N_2 and SF_6 arcs under a free recovery condition after a dc 50 A steady state condition. The temperature is expressed by a logarithmic colour scale. The configuration of the nozzle and electrodes is the same as that in the experiment, as presented in figure 3. Figure 21(a) depicts results for a CO_2 arc with 0.884 m/s gas introduction. It is readily apparent that the arc temperature decreases with time. Furthermore, a decrease rate in the arc temperature is greater around the nozzle throat, especially just at the nozzle throat inlet. Figure 14(b) shows that this calculated result agrees well with the time evaluation in the radiation intensity from CO_2 arcs. This rapid decay in the temperature around the nozzle throat inlet is attributable to high convection loss $\rho C_{\mathrm{p}} \boldsymbol{u} \cdot \nabla T$ there because the gas flow velocity $\boldsymbol{u}$ is high and the radial temperature gradient ∇T is higher than at other positions. This high radial temperature gradient arises from the cooling gas flow supplied to the nozzle throat inlet. In addition, the calculated results for 1.768 m/s CO_2 gas introduction are found in figure 21(b). In this case, the arc temperature starts decreasing around the nozzle throat, exhibiting a more rapid decrease in the temperature at 1.768 m/s than at 0.884 m/s. Results showed further that the experimentally obtained results of the radiation intensity from a CO_2 arc with 1.768 m/s gas introduction in figure 14(a) seems to decay more rapidly than those predicted by the present numerical simulation in figure 21(a). Perhaps this is true because turbulent flow effects are not considered in the calculation model.

Figure 21(c) presents calculated results for a N_2 arc with 1.768 m/s gas introduction. The calculation model predicts that a N_2 arc also decays from the nozzle throat inlet. This calculated transient temperature distribution closely resembles the experimentally observed result depicted in figure 15(b), from viewpoints of the arc decaying spatial position. Therefore, the present LTE model can predict arc behaviour with validity because N_2 arcs are quite stable during both steady state and decay without turbulent effects etc. in the experiment.

However, a difference exists between the calculated result and the observed result for SF_6 arcs. Figure 21(d) represents the results for a SF_6 arc with inlet flow velocity

of 1.768 m/s. The simulation predicts that SF_6 arc decays remarkably fast around the nozzle throat inlet because of a strong convection loss by cold and heavy SF_6 gas. This rapid decay in SF_6 arc temperature is attributed to the high convection loss caused by high specific heat, and high thermal conduction loss. The high specific heat and high thermal conductivity of SF_6 is involved equivalently by dissociation reactions of mainly SF_6, SF_4 and SF_2. This simulated temperature distributions shows a reasonably fast decay of the SF_6 arc, comparing with the observation result presented in figure 13(a). However, a difference between them remains. In the experiment, SF_6 actually produces strong turbulent flow, which makes the arc fluctuate. Furthermore, the actual SF_6 arc process is under a chemically non-equilibrium condition in which dissociation/ association reactions take finite time. Such turbulent effects and non-equilibrium effect should be considered in future work. In other words, the present comparison between the experimentally obtained results and the LTE simulated results are useful to ascertain the importance of these effects.

5.3. Influence of holes in the nozzle for LTS on arc behaviour

LTS measurements were done using a nozzle with a laser path hole and an observation hole. The observation hole was covered by a glass plate to prevent hot gas ejection from the nozzle throat, as described in the previous section. However, the current interruption test was conducted using nozzles with and without the holes. It is therefore necessary to confirm the influence of the presence of these holes in the nozzle on the arc behaviour.

Figure 22 shows the averaged arc voltage in a steady state in various gas conditions for the nozzles of the two types. One bar stands for results for the nozzle without the holes. The other bar shows results for the nozzle with holes for LTS measurement. The arc voltage measured from the time -5 ms to 0 ms was averaged for each gas condition. Each error bar is produced by at least 6 samples except a case of O_2 without a hole. As this figure shows, effects of the hole presence on the arc behaviours were not significant for all gases examined in this study. Except for SF_6, the arc voltage is slightly lower with the holes. Consequently, the influences of the hole presence might be neglected in the present work.

6. Conclusions

This paper presents current interruption capabilities of various gas quantified using a newly developed method. The method uses an insulated gate bi-polar transistor (IGBT) as a current and voltage control device. SF_6, CO_2, O_2, N_2, air and Ar arcs in DC current of 50 A were ignited in a gas-flow nozzle, after which they decayed because of the current commutation to the IGBT parallel connected to the arcing electrodes. After specified delay time t_d from initiation of the arc decaying, a steep voltage was intentionally applied to the electrodes. A case in which the arc did not re-ignite is regarded as successful interruption. The probability of successful interruption was investigated statistically for

every gas. Consequently, SF_6 was estimated as taking 28 μs to have 50% probability of successful interruption ($t_{d50\%} = 28$ μs): the fastest of these gases. Also, $t_{d50\%}$ of CO_2 was 108 μs. $t_{d50\%}$ of N_2 was 240 μs. In this way, current interruption capabilities of various gases can be evaluated quantitatively using the developed method. Furthermore, arc behaviour in a steady state and decaying phase were observed using a high-speed video camera. The electron density of the residual arc in decaying phase was measured using LTS method. Comparison between arc behaviour and the electron density showed good agreement. No contradiction was found with results of current interruption tests.

Results obtained in this work will support consideration of the fundamental characteristics of arc discharge and development of alternatives to SF_6. Additional approaches must be made to ascertain the fundamental properties of current interruption phenomena. We are planning further investigation such as the influence of TRV peak voltage and rise rate using advanced technique with power semiconductors.

References

[1] Cressault Y, Connord V, Hingana H, Teulet P and Gleizes A 2011 Transport properties of CF_3I thermal plasmas mixed with CO_2, air or N_2 as an alternative to SF_6 plasmas in high-voltage circuit breakers *J. Phys. D: Appl. Phys.* **44** 495202 (22pp)

[2] Wang W, Rong M, Wu Y and Yan J D 2014 Fundamental properties of high-temperature SF_6 mixed with CO2 as a replacement for SF_6 in high-voltage circuit breakers *J. Phys. D: Appl. Phys.* **47** 255201 (16pp)

[3] Yang A, Liu Y, Sun B, Wang X, Cressault Y, Zhong L, Rong M, Wu Y and Niu C 2015 Thermodynamic properties and transport coefficients of high-temperature CO_2 thermal plasmas mixed with C_2F_4 *J. Phys. D: Appl. Phys.* **48** 495202 (25pp)

[4] Sun Hao, Rong M, Wu Y, Chen Z, Yang F, Murphy A B and Zhang H 2015 Investigation on critical breakdown electric field of hot carbon dioxide for gas circuit breaker applications *J. Phys. D: Appl. Phys.* **48** 055201 (16pp)

[5] Kieffel Y, Biquez F and Ponchon P 2015 Alternative gas to SF_6 for use in high voltage switchgears: g^3 *23rd International Conference on Electricity Distribution* Paper0230

[6] Hyrenbach M, Hintzen T, Müller and Owens J 2015 Alternative gas insulation in medium-voltage switchgear *Proc. 23rd Int. Conf. on Electricity Distribution*, paper0587

[7] Murai K, Nakano T, Tanaka Y, Uesugi Y, Ishijima T, Tomita K, Suzuki K, Iijima T and Shinkai T 2016 The LTE thermofluid simulation of Ar/SF_6 gas-blast arcs in a nozzle space in an arc device *IEEJ Trans. PE* **136**(9) pp.741-748

[8] Sun H, Tanaka Y, Tomita K, Wu Y, Rong M, Uesugi Y and Ishijima T 2015 Computational non-chemically equilibrium model on the current zero simulation in a model N_2 circuit breaker under the free recovery condition *J. Phys. D: Appl. Phys.* **49** 055204 (17pp)

[9] Kamimae R, Tanaka Y, Uesugi Y, Ishijima T and Shinkai T 2012 Observation of decaying arc behaviors in Ar and Ar/SF_6 gas confined in a nozzle using a high speed video camera *Joint Conference of IWHV 2012 & JK 2012 on ED & HVE* ED-12-147, SP-12-074, HV-12-077

[10] Tomita K, Gojima D, Nagai K, Uchino K, Kamimae R, Tanaka Y, Suzuki K, Iijima T, Uchii T and Shinkai T 2013 Thomson scattering diagnostics of decay processes of Ar/SF_6 gas-blast arcs confined by a nozzle *J. Phys. D: Appl. Phys.* **46** 382001 (5pp)

[11] Tomita K, Gojima D, Shimizu T, Uchino K, Nakano T, Tanaka Y, Suzuki K, Iijima T and Shinkai T 2015 Thomson scattering diagnostics of SF_6 gas-blasted arcs confined by a nozzle under free-recovery conditions *J. Phys. D: Appl. Phys.* **48** 265201 (14pp)

[12] Inada Y, Kumada A, Ikeda H, Hidaka K, Nakano T, Murai K, Tanaka Y and Shinkai T 2017

Comparative study on extinction process of gas-blasted air and CO_2 arc discharge using two-dimensional electron density imaging sensor *J. Phys. D: Appl. Phys.* **50** 175202

[13] Tanaka Y, Nakano T, Shimizu T, Tomita K and Fujino T and Suzuki K 2015 Fundamental Investigation Technique on Gas-Blast Arc Behaviors in Decaying Re-ignition Processes using Power Semiconductors *Trans.IEEJ* **135**(1) pp.1-8

[14] Nakano T, Murai K, Tanaka Y, Uesugi Y, Ishijima T, Shiraishi T, Shimizu T, Tomita K, Suzuki K and Shinkai T 2015 Evaluation on Current Interruption Ability of CO_2 and SF_6 using Current and Voltage Application Highly Controlled by Power Semiconductors *3rd International Conference on Electric Power Equipment - Switching Technology ICEPE-ST2015 (Busan, Korea)* GO-438

[15] Nakano T, Murai K, Tanaka Y, Uesugi Y, Ishijima T, Shiraishi T, Shimizu T, Tomita K, Suzuki K and Shinkai T 2016 Evaluation on Current Interruption Ability of Various Gases using Current and Voltage Application Highly Controlled by Power Semiconductors *21th International Conference on Gas Discharges and their Applications GD2014 (Nagoya, Japan)* A25 pp.97-100

[16] Muraoka K and Kono A 2011 Laser Thomson scattering for low-temperature plasmas *J. Phys. D: Appl. Phys.* **44** 043001 (15pp)

[17] Tanaka Y, Yamachi N, Matsumoto S, Kaneko S, Okabe S, Shibuya M 2008 Thermodynamic and Transport Properties of CO_2, CO_2-O_2, and CO_2-H_2 Mixtures at Temperatures of 300 to 30,000 K and Pressures of 0.1 to 10 MPa *Electrical Engineering in Japan* **163**(4) pp.18-29

[18] Tanaka Y, Paul K C, Sakuta T 2000 Thermodynamic and Transport Properties of N_2/O_2 Mixtures at Different Admixture Ratios *Trans.IEEJ* **120-B**(1) pp.24-30

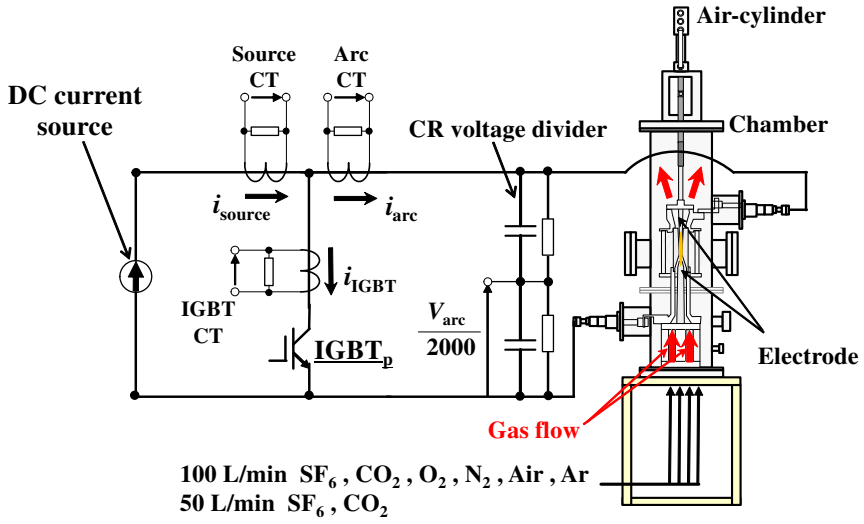

Figure 1. Schematic of the experimental electric circuit.

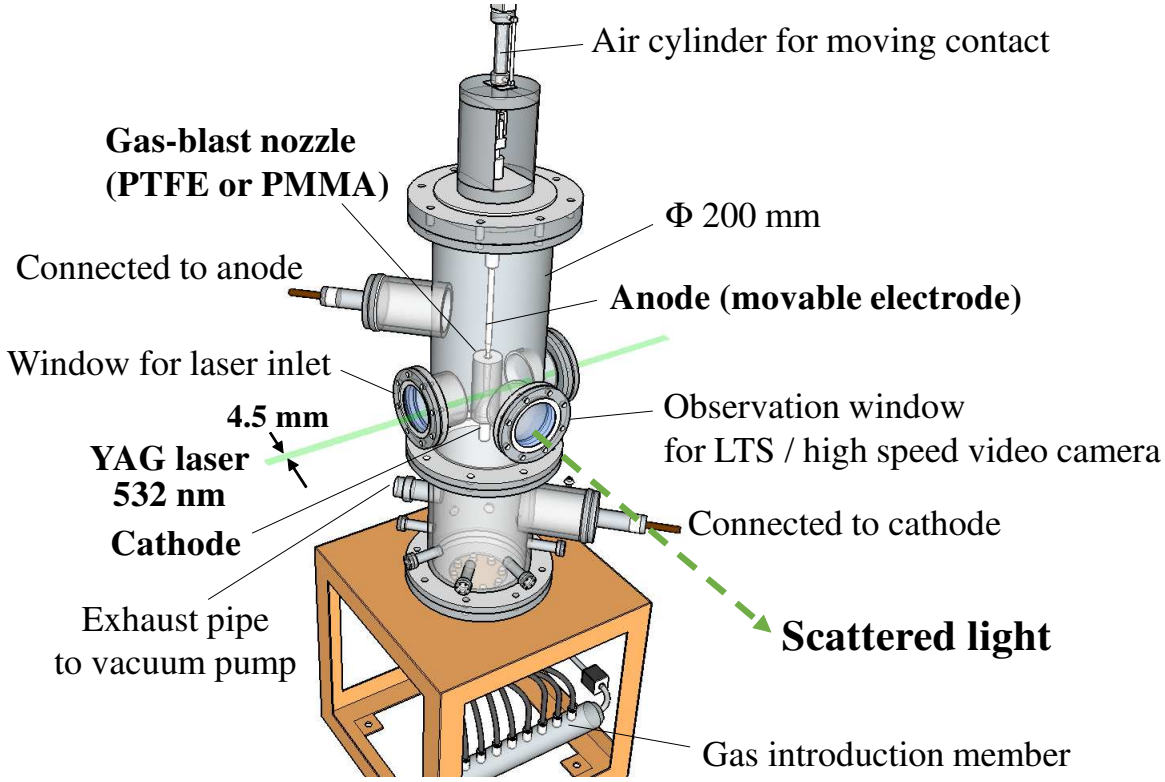

Figure 2. Experimental arc device.

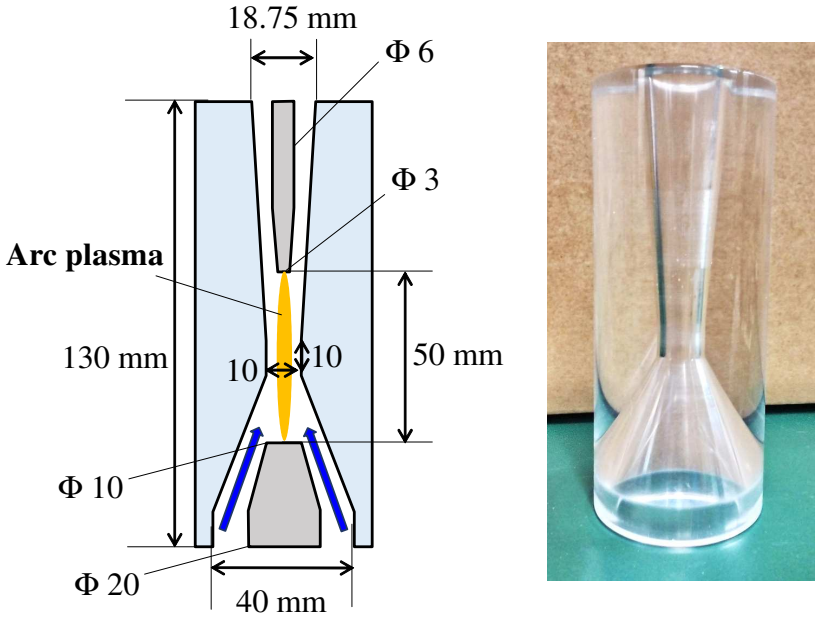

Figure 3. Schematic diagram of a gas-blast nozzle and a photograph of a PMMA transparent nozzle.

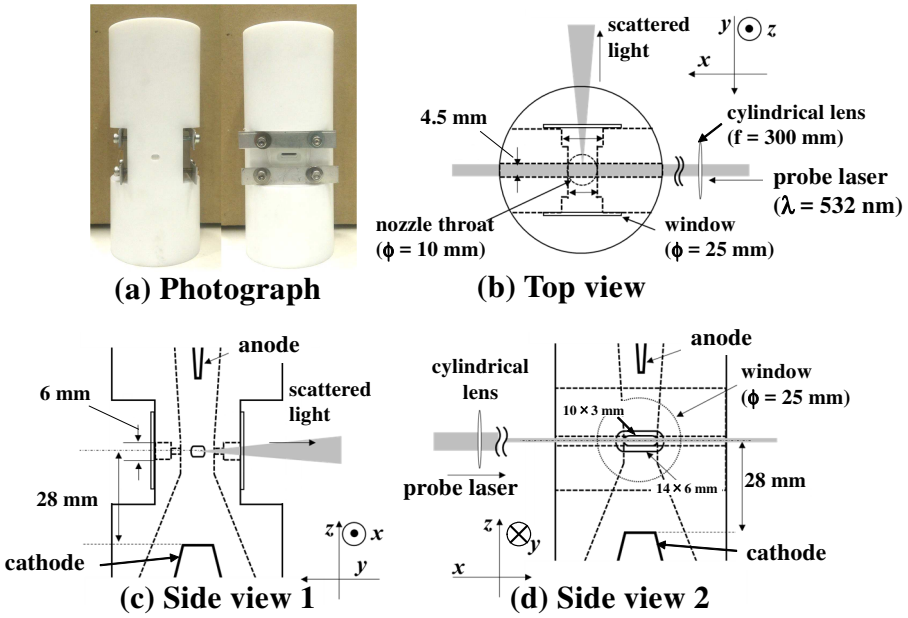

Figure 4. PTFE nozzle for electron density measurement using laser Thomson scattering (LTS): (a) photograph of the PTFE nozzle from both sides, (b) top view of the cross section of the nozzle, (c) view from the laser inlet side, and (d) view from the observation side.

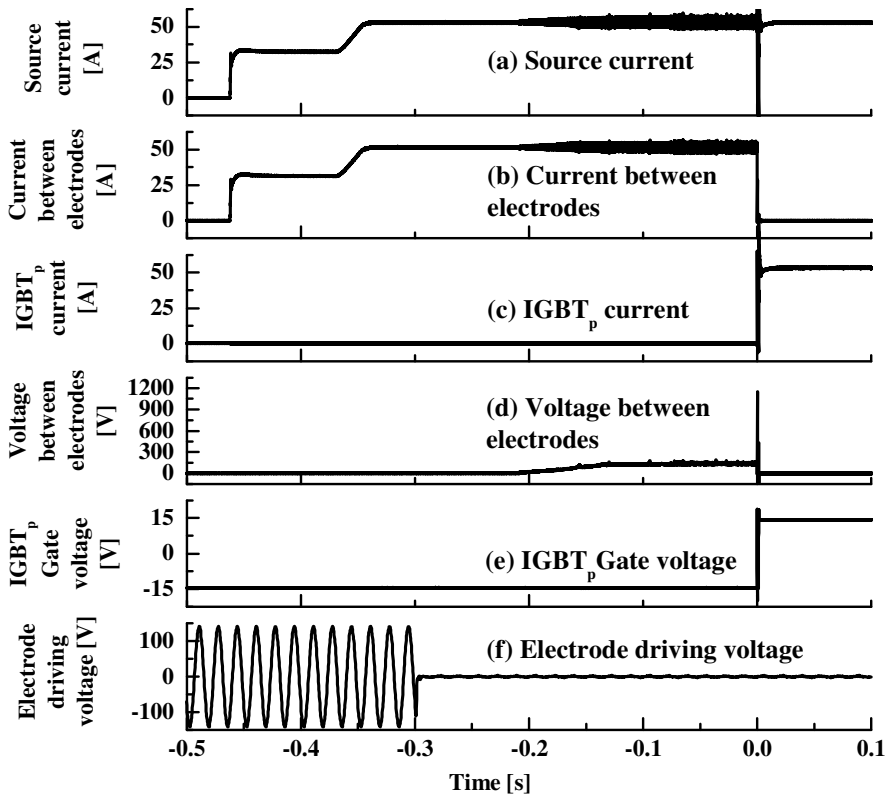

Figure 5. Example of measured current and voltage waveforms through one experimental shot.

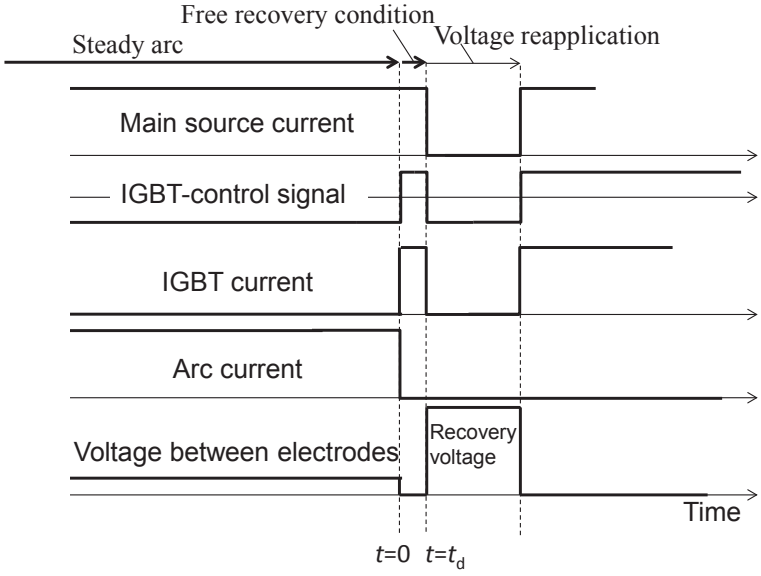

Figure 6. Conceptual current and voltage behaviours in cases of success of arc interruption after quasi-transient recovery voltage application.

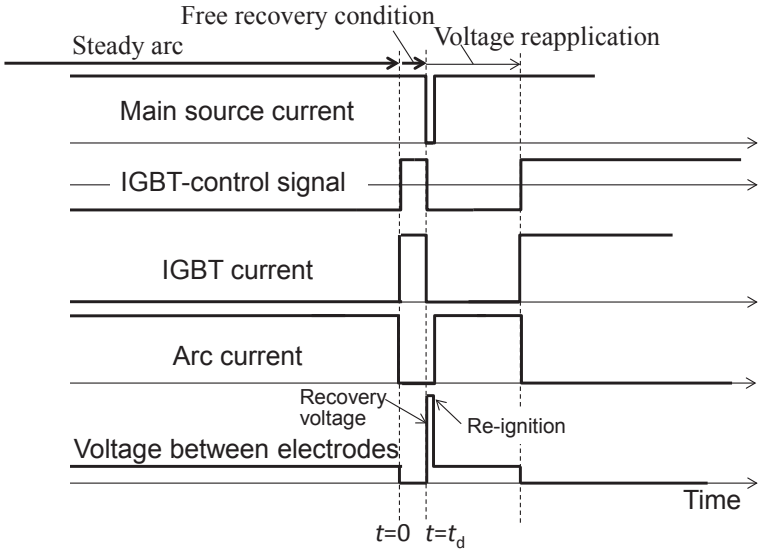

Figure 7. Conceptual current and voltage behaviours in cases of arc re-ignition after quasi-transient recovery voltage application.

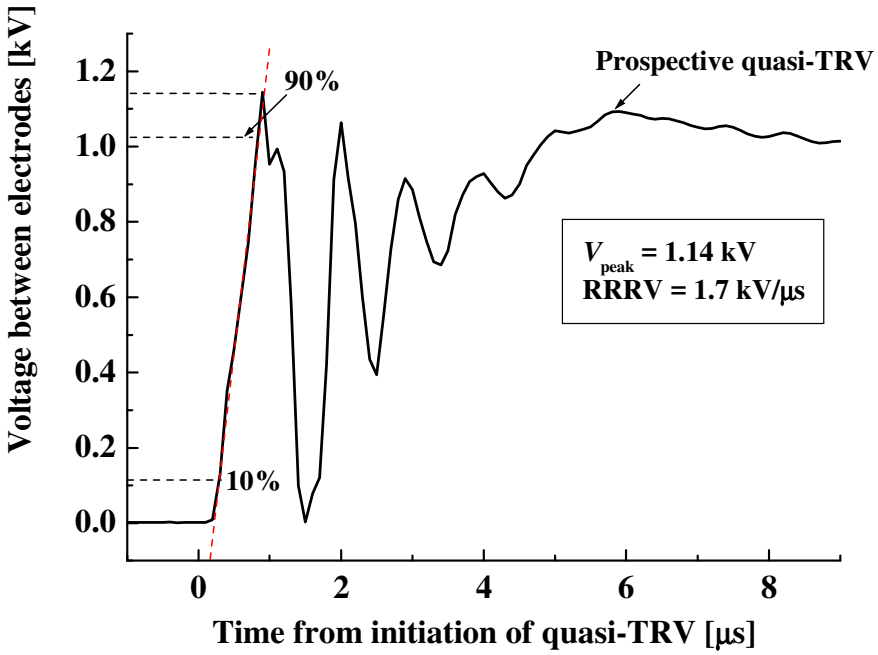

Figure 8. Waveform of prospective quasi-transient recovery voltage (quasi-TRV).

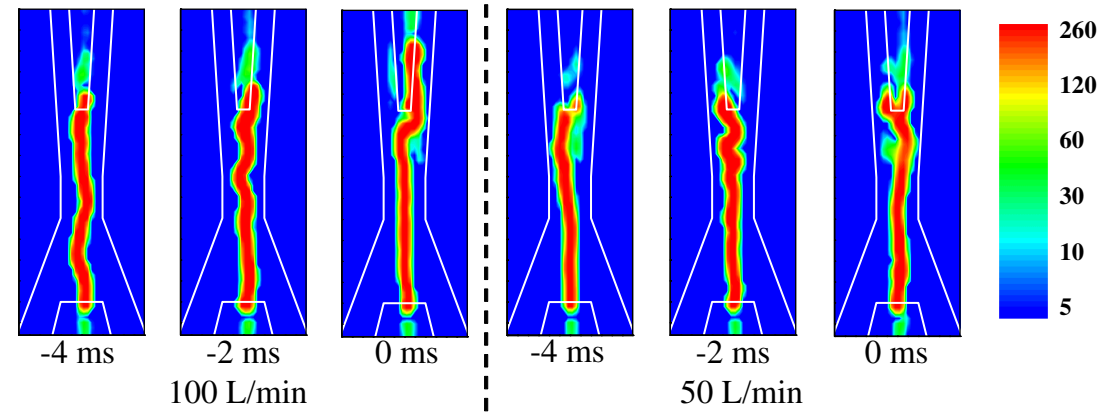

(a) SF_6

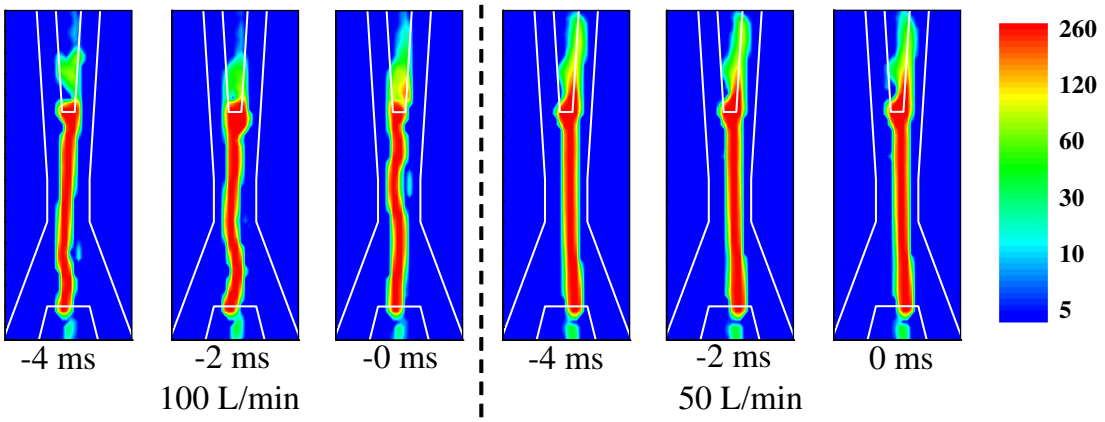

(b) CO_2

Figure 9. Arc behaviour in a steady state before free recovery condition in (a) SF_6 and (b) CO_2 with 100 and 50 L/min flow rates (logarithmic scale colour map).

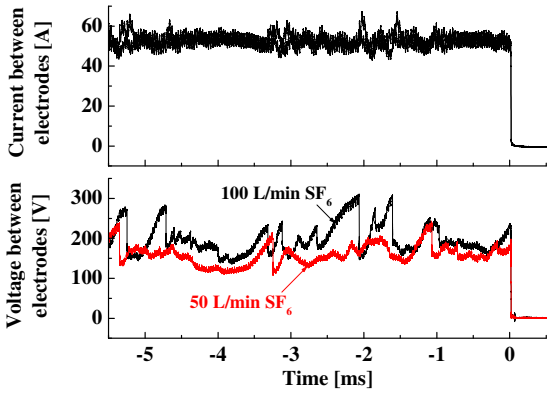

(a) SF_6

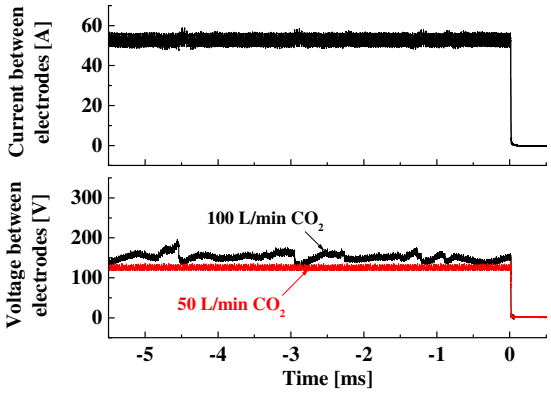

(b) CO_2

Figure 10. Arc current and voltage waveforms in a steady state before the free recovery condition in (a) SF_6 and (b) CO_2 with 100 L/min and 50 L/min flow rates.

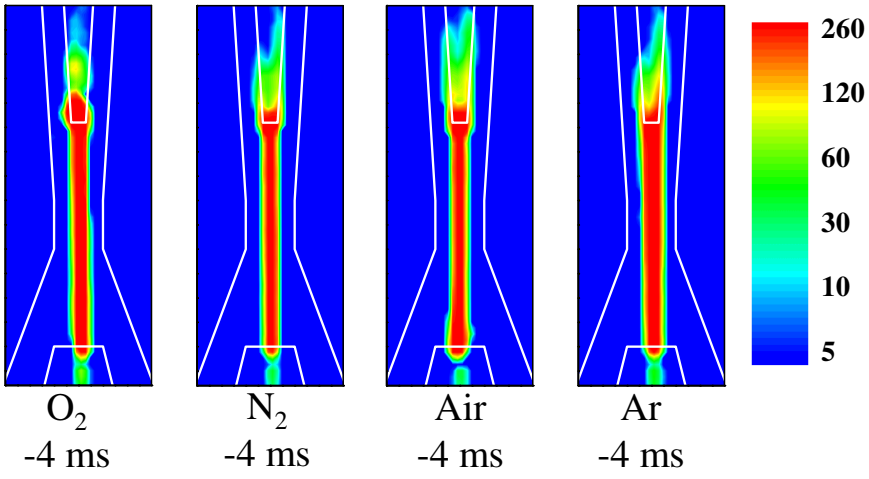

Figure 11. Arc behaviour in a steady state in O_2, N_2, air and Ar with a 100 L/min flow rate (logarithmic scale colour map).

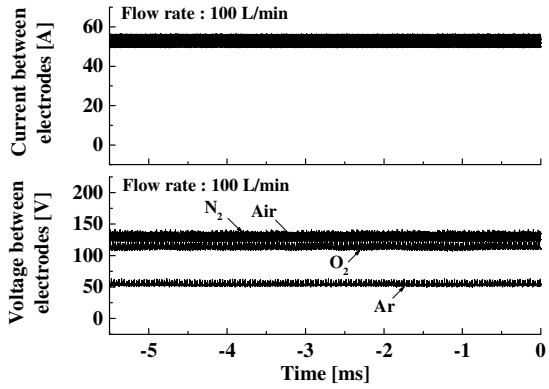

Figure 12. Arc current and voltage waveforms in a steady state in O_2, N_2, air and Ar with a 100 L/min flow rate.

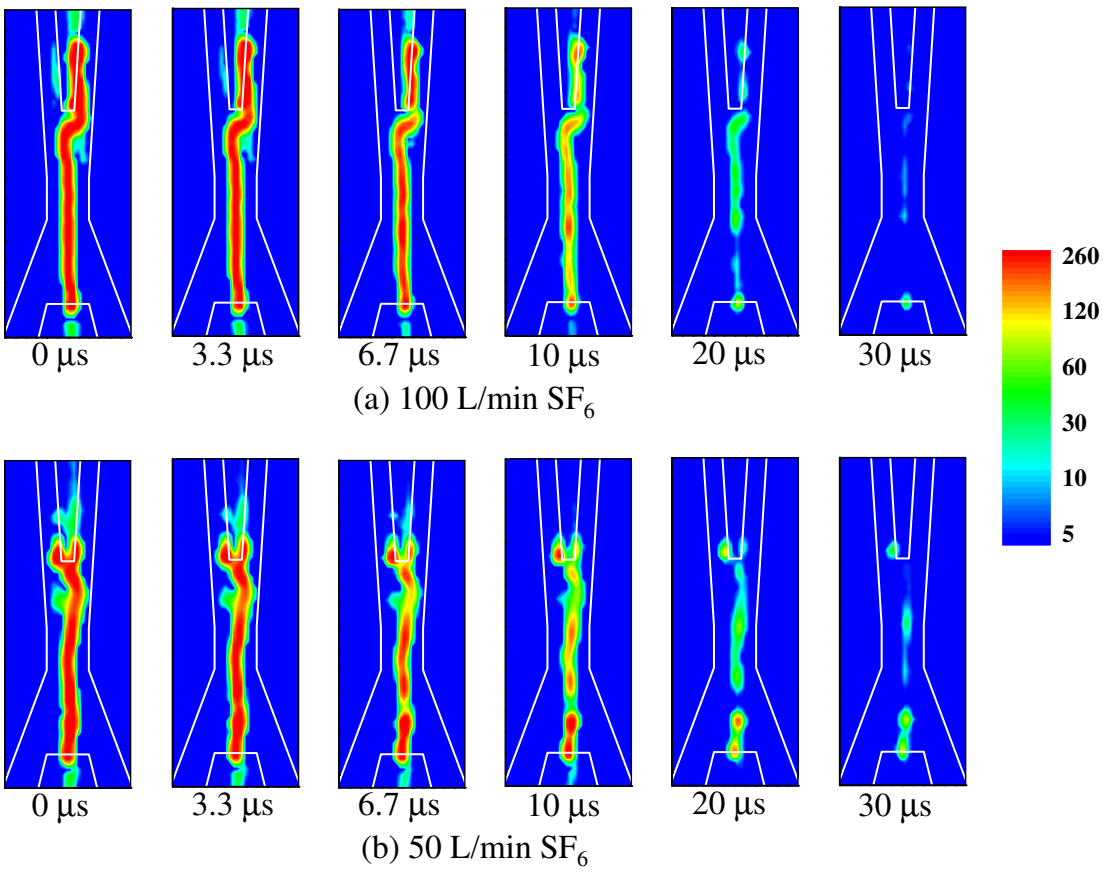

Figure 13. Arc behaviour in decaying phase in SF_6 with 100 and 50 L/min flow rates (logarithmic scale colour map).

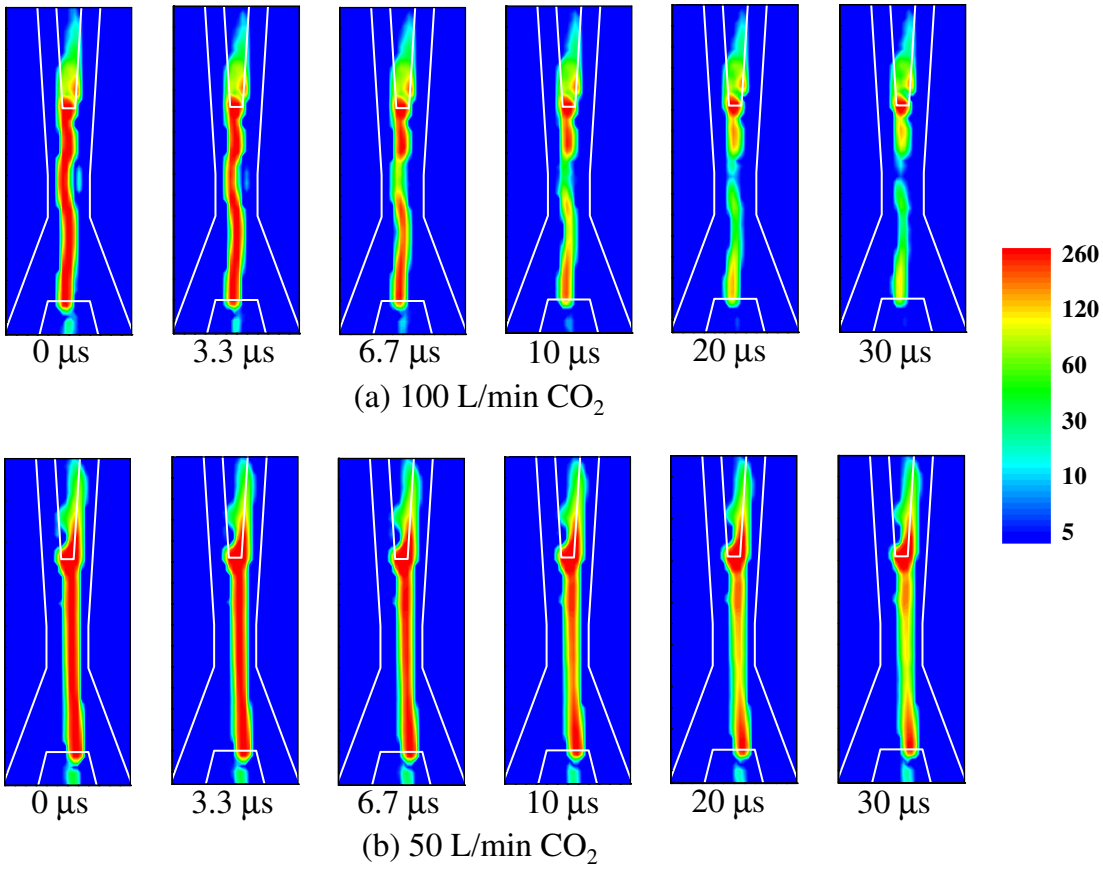

Figure 14. Arc behaviour in decaying phase in CO_2 with a 100 or 50 L/min flow rate (logarithmic scale colour map).

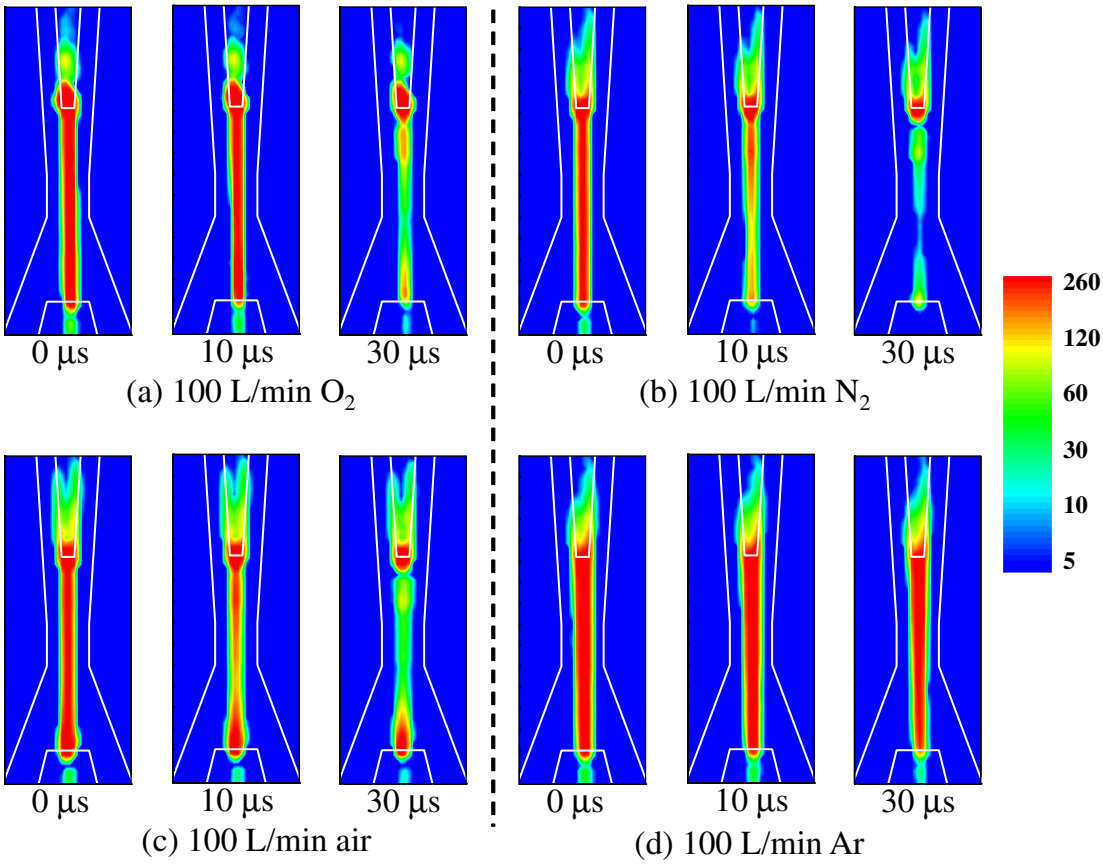

Figure 15. Arc behaviour in decaying phase in O_2, N_2, air and Ar with a 100 L/min flow rate (logarithmic scale colour map).

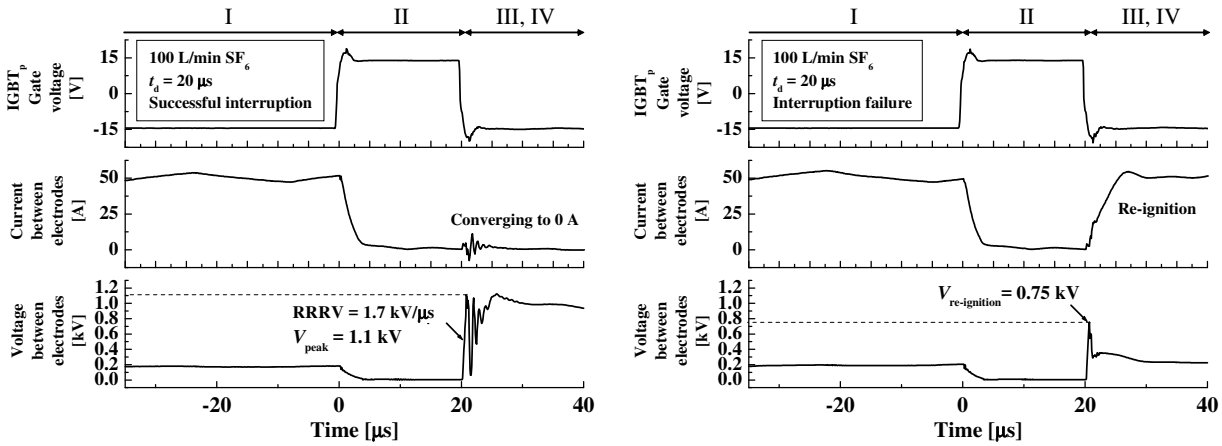

Figure 16. Examples of measured current and voltage waveforms around a quasi-TRV application.

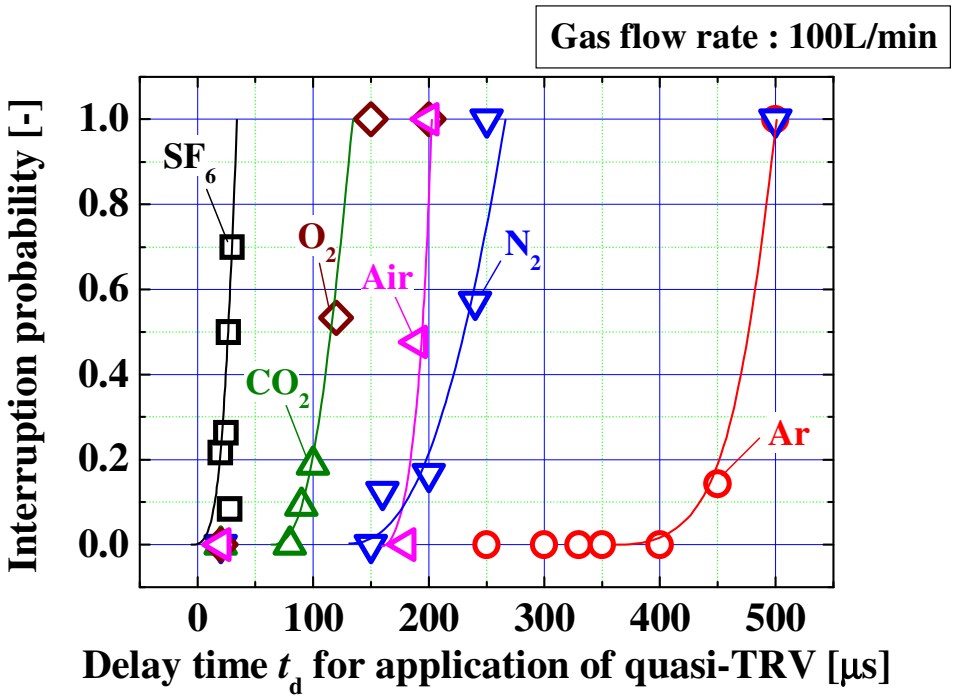

Figure 17. Probability of successful interruption versus voltage application delay time t_{d} for cases with a 100 L/min gas flow rate.

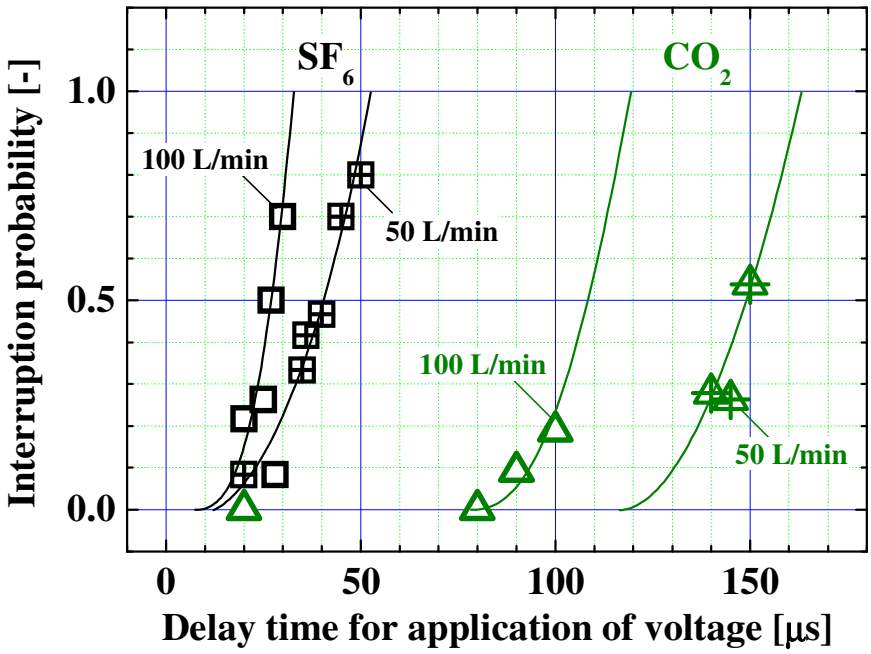

Figure 18. Probability of successful interruption versus voltage application delay time t_{d} for the cases of SF_6 and CO_2 at 50 and 100 L/min flow rates.

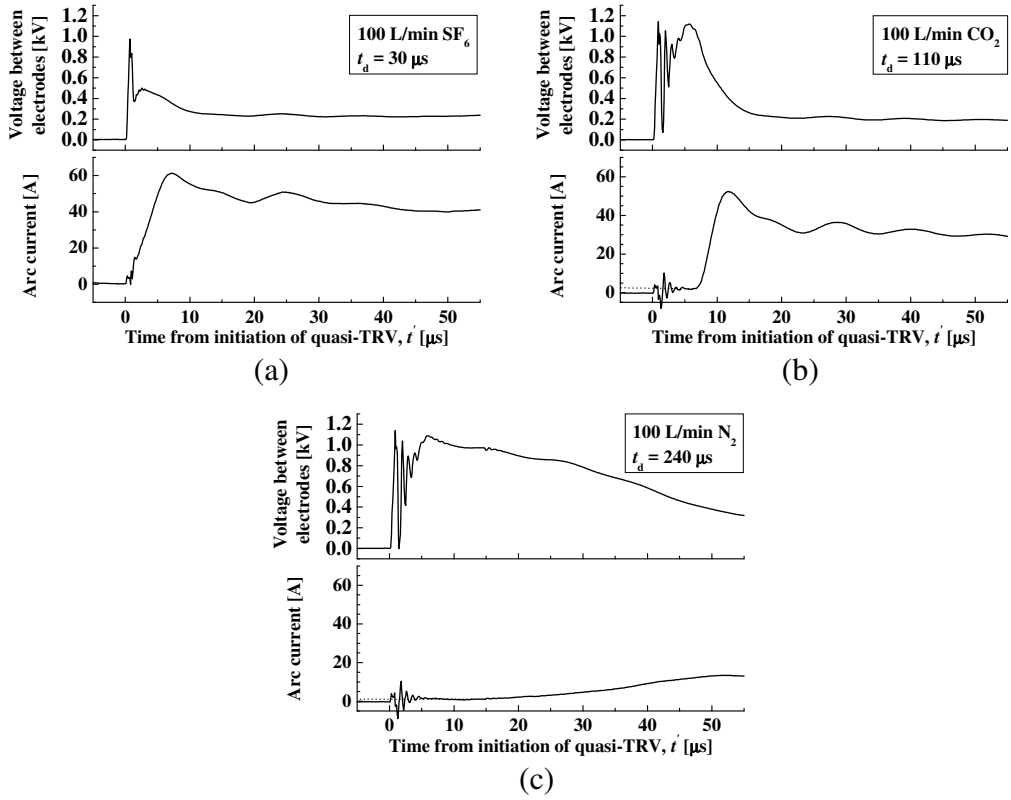

Figure 19. Waveforms of current and voltage on interruption failure for SF_6, CO_2, and N_2 at a 100 L/min flow rate.

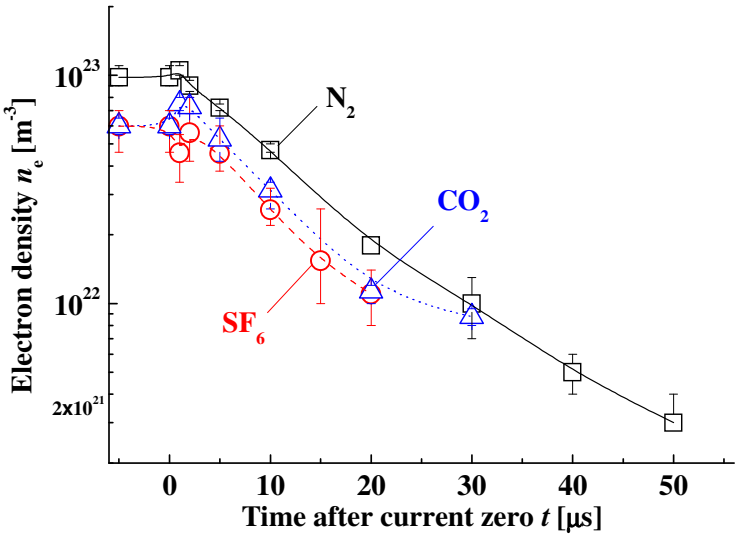

Figure 20. Time evolution in the electron density in SF_6, CO_2 and N_2 arcs after current reduction to zero.

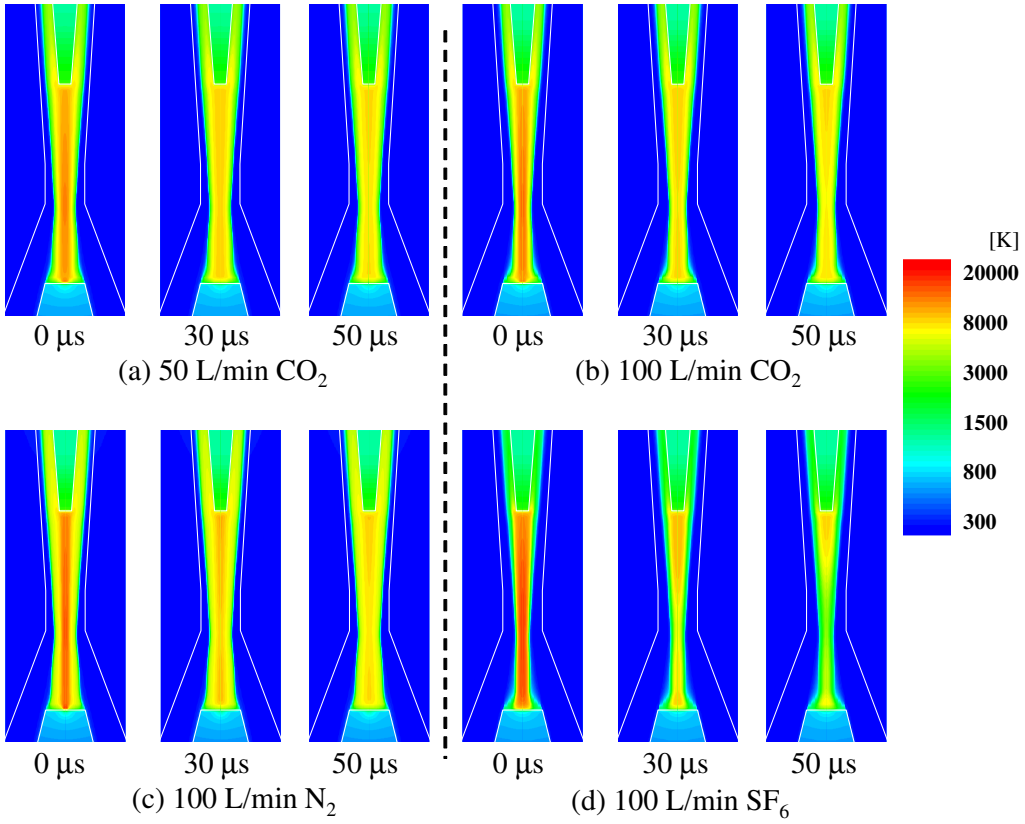

Figure 21. Simulated time variation of the two-dimensional temperature distribution of CO_2, N_2 and SF_6 arcs in the decaying process.

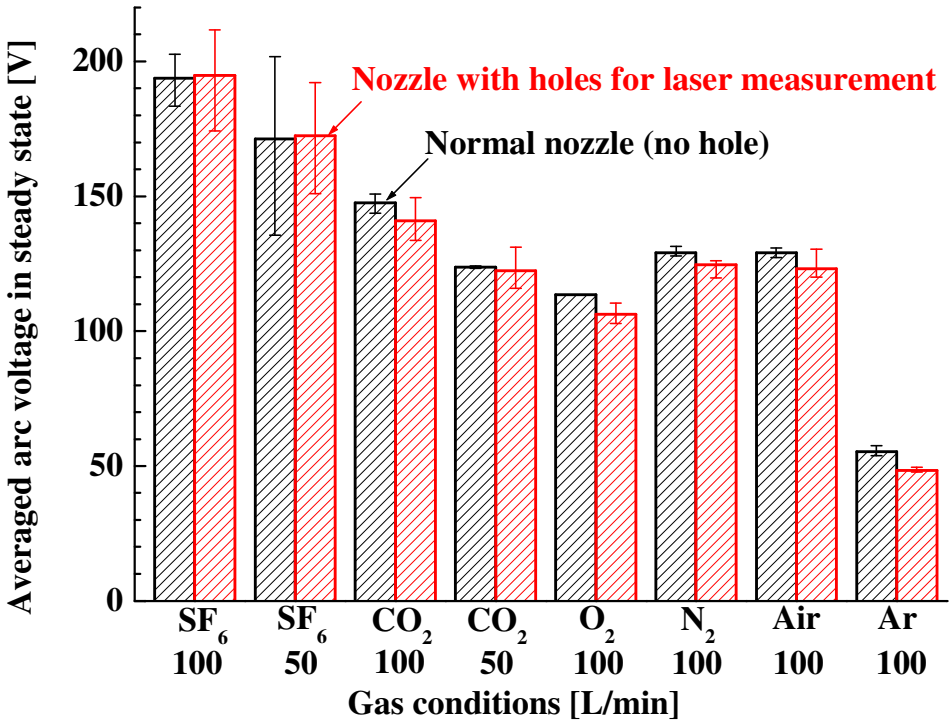

Figure 22. Averaged arc voltage in a steady state in various gas conditions.